J Mater Sci (2017) 52:6976–6986

Electrochemically induced Ti^{3+} self-doping of TiO_2 nanotube arrays for improved photoelectrochemical water splitting

Jingnan Song[1], Maojun Zheng[1,2,*], Xiaoliang Yuan[3], Qiang Li[1], Faze Wang[1], Liguo Ma[1], Yuxiu You[1], Shaohua Liu[4], Pengjie Liu[1], Dongkai Jiang[1], Li Ma[5], and Wenzhong Shen[1]

[1] *Key Laboratory of Artificial Structure and Quantum Control, Ministry of Education, Department of Physics and Astronomy, Shanghai Jiao Tong University, Shanghai 200240, People's Republic of China*
[2] *Collaborative Innovation Center of Advanced Microstructures, Nanjing 210093, People's Republic of China*
[3] *Research Institute of Criminal Science and Technology, 803 Zhongshan Beiyi Road, Shanghai, People's Republic of China*
[4] *Department of Chemistry and Food Chemistry, Center for Advancing Electronics Dresden (cfaed), 01062 Dresden, Germany*
[5] *School of Chemistry and Chemical Technology, Shanghai Jiao Tong University, Shanghai 200240, People's Republic of China*

Received: 1 December 2016
Accepted: 16 February 2017
Published online: 27 February 2017

ABSTRACT

We report a facile electrochemical reduction method to synthesize Ti^{3+}-self-doped TiO_2 nanotube arrays (TNTs), where the effects of reduction duration and potential on the photoelectrochemical performance were systematically investigated. The X-ray photoelectron spectroscopy and electron paramagnetic resonance spectra confirmed the presence of Ti^{3+} in the TNTs. Under the optimum reduction condition, the Ti^{3+}-self-doped TNTs exhibited remarkably enhanced photocurrent density and photoconversion efficiency, which were nearly 3.1 and 1.75 times that of pristine TNTs, respectively. The enhancement of PEC performance is due to the improved electrical conductivity, accelerated charge transfer rate at the TNTs/electrolyte interface, as well as the improved visible light response, which is elucidated by electrochemical impedance spectra, Mott–Schottky, and UV–Vis diffuse reflection spectra.

Introduction

Solar-driven photoelectrochemical (PEC) water splitting is one of the most promising pathways for converting solar energy into useable energy since both water and sunlight are abundant on the earth. Since the first report on the realization of PEC water splitting using TiO_2 electrodes in 1972 [1], numerous semiconductor materials have been extensively investigated as photoelectrodes in PEC system [2–4], among which TiO_2 nanotube arrays (TNTs) have attracted the most attention due to its chemical and photochemical stability, high specific surface area, low cost, and non-toxic. However, the intrinsically large band gap of TNTs (i.e., 3.2 eV for anatase and 3.0 eV for rutile) limits its photoresponse only in

Address correspondence to E-mail: mjzheng@sjtu.edu.cn

DOI 10.1007/s10853-017-0930-z

ultraviolent (UV) light region, which is only 4% of the solar spectrum. Moreover, the intrinsic fast electron–hole recombination owing to its poor electrical conductivity is also a limitation.

To address these problems, much effort has been made to enhance the PEC performance of TNTs by extending the spectra absorption into the visible region. Recent works have focused on the doping of nonmetals or metals (N, F, Cr, and Sb) into TNTs crystal lattice [5–8]. The hetero-element doping can induce new energy levels located near the band edges or as mid-gap states, thus narrowing the band gap of TNTs. Although the incorporation of foreign elements can promote its visible light photocatalytic activity, it inevitably causes more structural defects, which undesirably lead to increased carrier recombination centers. In view of the inherent drawbacks of hetero-element doping approach, Ti^{3+} self-doping has drawn much attention recently and been especially regarded as a very promising strategy to enhance PEC performance of TiO_2 [9–12].

Several synthesis routes including hydrogen thermal treatment [13–16], hydrogen or argon plasma treatment [17, 18], and chemical reduction [11, 19–22] were developed to prepare self-doped TNTs. Chen et al. [23] reported the preparation of black TiO_2 nanoparticles by treating white TiO_2 nanoparticles under high-pressure pure hydrogen atmosphere, which shows a broadened optical absorption from UV region to NIR region (~1200 nm). However, the harsh reduction conditions such as high pressure, dangerous H_2 gas, high vacuum, and long treatment time (120 h) is less suitable for practical application. Recently, Zhu et al. [19] synthesized black brookite TiO_2 nanoparticles in a two-zone vacuum furnace with the Al reduction method. Yet high temperature (800 °C for producing Al vapor and 300–600 °C for the reaction) and long reaction time (4 h) were still required.

In this context, it is of great significance to develop a safer and effective reduction method. Recently, electrochemical reduction method has proved to be promising for preparing reduced TNTs, and three different reduction electrolytes have been developed, including acidic (H_2SO_4) [24], neutral (Na_2SO_4) [11], and alkaline (KOH) aqueous solution [25]. In Close's report [25], Ti^{3+} self-doping TNTs were obtained by reducing pure TNTs in two different types of solutions (acidic or alkaline solution). Its results showed that TNTs reduced in alkaline solution (KOH aqueous solution with a pH of 13) exhibited improved oxygen scavenging performance compared with that prepared in acidic solution. During reduction in acidic solution (pH = 3), vigorous bubbling is observed on both cathode and anode, which suggests that most of the reactions occurring are gas-forming side reactions. Hence, acidic solutions appear to be ill-suited for the selective reduction of TiO_2, while alkaline solutions show a good selectivity toward the desired oxide reduction. So far, there has been a lack of systematic investigation on the PEC performance of TNTs reduced in KOH aqueous solution.

Here, we report the preparation of Ti^{3+}-self-doped TNTs by controllable electrochemical reduction in a three-electrode configuration. With this approach, a series of reduced TNTs have been synthesized by changing the reduction duration and potential, and then its PEC properties have been investigated in detail. Among these samples, the optimal photocurrent density is up to 0.525 mA cm^{-2} (vs Ag/AgCl), which is about 3.1 times that of pristine TNTs (0.170 mA cm^{-2}). By combining the diverse characterization techniques, electrochemical impedance spectra and Mott–Schottky plots, a possible explanation for the enhanced PEC performance is proposed.

Experimental details

Preparation of TNTs

Prior to anodization, titanium (Ti) foil (99.7% purity, 0.1 mm thickness) was degreased by successively sonicating in acetone and ethanol for 10 min to remove contaminants followed by a chemical polishing in an aqueous solution containing $HF/HNO_3/H_2O$ with a volume ratio of 1:3:6 for 30 s. Then it was rinsed with deionized (DI) water and dried in a nitrogen stream. The anodization was carried out in a two-electrode configuration with graphite plate as cathode and Ti foil as anode. All electrolytes consisted of 0.3 wt% ammonium fluoride (NH_4F), 96 vol% ethylene glycol (EG), and 4 vol% DI water. In the first step anodization, the Ti foil was anodized at 90 V for 60 min, and then the as-grown nanotube arrays was ultrasonically removed in 0.1 M HCl aqueous solution. Then the same Ti foil underwent a second anodization at 90 V for 5 min. After the two-step anodization, the prepared TNTs were annealed

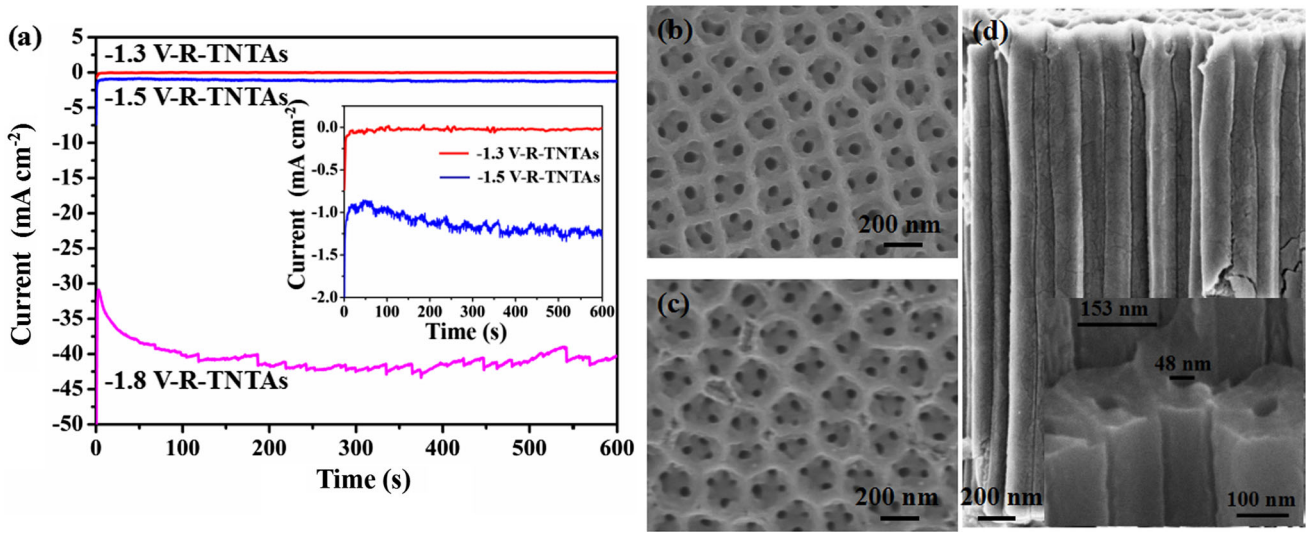

Figure 1 TNTs before and after electrochemical reduction. **a** Dependence of reduction current on time at cathodic potentials of −1.3, −1.5, and −1.8 V (vs Ag/AgCl) (*inset* magnified reduction current of −1.3 V-R-TNTs and −1.5 V-R-TNTs). **b** *Top view* of pristine TNTs. *Top view* (**c**) and *side view* (**d**) of −1.5 V-R-TNTs. The *inset* in **d** shows the magnified *side view* of −1.5 V-R-TNTs.

in air at 450 °C for 2 h with a heating rate of 2 °C min^{-1}.

Preparation of Ti^{3+}-self-doped TNTs

The electrochemical reduction was performed in a three-electrode system with the TNTs as working electrode, Pt mesh as counter electrode, and Ag/AgCl as reference electrode. The supporting electrolyte was 1 M KOH aqueous solution (pH = 13.6). In this step, electrochemical reduction was conducted at different cathodic potentials (−1.3, −1.5, and −1.8 V) for different duration (5, 10, and 20 min). The Ti^{3+}-self-doped TNTs prepared at different potentials for 10 min are denoted as X-R-TNTs (X = −1.3, −1.5, and −1.8 V), while reduced TNTs at −1.5 V for different times are denoted as R-TNTs-X (X = 5, 10, and 20 min).

Characterization

The morphology of TNTs before and after electrochemical reduction was examined using field-emission scanning electron microscope (SEM, Zeiss Ultra Plus FESEM). The crystal structure and phase of samples were determined by X-ray diffraction (XRD, D8 ADVANCE X-ray diffractometer, Bruker, Germany), with incidence angles ranging from 20° to 80°. The surface composition of samples was analyzed by X-ray photoelectron spectroscopy (XPS, AXIS ULTRA DLD, Kratos, Japan) using monochromatic Al Kα as the X-ray source (150 W). The binding energy was calibrated to 284.6 eV using the C1 s photoelectron peak as the reference. Electron paramagnetic resonance spectra (EPR) were collected at 103 K on a Bruker EMX-8/EPR spectrometer. The diffuse reflectance UV–Vis absorption spectra were recorded on a spectrophotometer (Lambda 950, PerkinElmer), with $BaSO_4$ as a reference.

PEC characterization of TNTs before and after electrochemical reduction

PEC measurement was performed in a three-electrode PEC cell with pristine TNTs and reduced TNTs as the working electrode, Pt mesh as the counter electrode, and Ag/AgCl as the reference electrode. An electrochemical workstation (PARSTAT 4000) instrument was used to measure the PEC properties of samples. 1 M KOH aqueous solution was used as the electrolyte. All three electrodes were put into a glass cell with a quartz window through which the working electrode was illuminated from the front sides by a solar simulator [SOLARDGE 700, a 300 W xenon arc lamp equipped with an air mass (AM 1.5 G filter)]. The incident illumination was adjusted to 100 mW cm^{-2} by changing the position of the lamp relative to that of the electrochemical cell. The

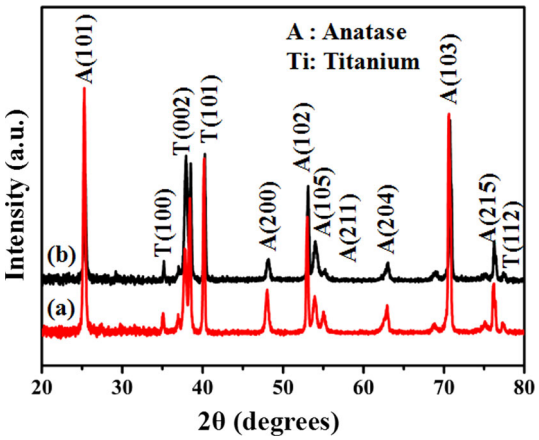

Figure 2 X-ray diffraction patterns of *a* pristine TNTs, *b* −1.5 V-R-TNTs.

photocurrent density–voltage linear sweep voltammetry (LSV) curves were measured under AM 1.5 G illumination. The transient photoresponse was evaluated under chopped light irradiation (light on–off cycles: 30 s). Potentials are reported as measured versus Ag/AgCl and as calculated versus RHE using the Nernstian relation $E_{RHE} = E_{Ag/AgCl} + 0.059\ pH + E^0_{Ag/AgCl}$ [26], where E_{RHE} is the converted potential versus RHE, $E_{Ag/AgCl}$ is the experimental potential measured against the Ag/AgCl reference electrode, and $E^0_{Ag/AgCl}$ is the standard potential of Ag/AgCl at 25 °C (0.1976 V). The applied bias photoconversion efficiencies (η) of the samples were calculated using the following equation: $\eta(\%) = I(E^0_{rev} - V)/J_{light}$ [11], where I is the photocurrent density (mA cm^{-2}), J_{light} is the incident illumination power density (mW cm^{-2}), E^0_{rev} is the standard reversible potential (1.23 V vs RHE), and V is the applied bias potential versus RHE.

Electrochemical impedance spectroscopy was carried out to understand the charge transfer process between photoelectrodes/electrolyte interfaces. All the measurements were performed under the open-circuit condition with the frequency ranging from 0.01 Hz to 100 kHz. Mott–Schottky plots were measured in the dark at an AC frequency of 1.0 kHz.

Results and discussion

Figure 1a shows the dependence of reduction current on time at cathodic potentials of −1.3, −1.5, and −1.8 V (vs Ag/AgCl). At low cathodic potential (−1.3 V), the reduction current was so small that it may result in a low number of Ti^{3+} or oxygen vacancies [27], which can be confirmed by the following PEC performance of the samples. When the cathodic potential was raised to −1.5 V, a large stable current was yielded (~1.25 mA cm^{-2}). Further increasing the cathodic potential to −1.8 V produced a larger current of 42 mA cm^{-2}. The time dependence of the current at this potential is different from that at −1.5 V. Such high current is related not only to the reduction of the TNTs but also to the reduction of H^+ to H_2. The morphology of pristine TNTs and −1.5 V-R-TNTs is examined by SEM, shown in Fig. 1b–d. It can be observed that the compact and vertically aligned nanotube arrays were produced by the two-step anodization, with an average length of ~3.0 μm. The inner diameter and wall thickness are ~48 and ~52 nm, respectively. Compared with the pristine TNTs, the nanotube structures of reduced TNTs at −1.5 V are observed to be maintained, suggesting that the morphology of TNTs was stable and not undergoing any destruction under electrochemical reduction.

In this study, the TNTs were fabricated under the same anodization parameters. Thus, the specific area of all the samples is almost the same. Assuring the TNTs made up of hollow cylinders, the evolution of specific area (A) can be determined by the following equation:

$$A = 2\pi(r_i + r_o) \times l \times N_t \quad (1)$$

where r_i is the inner radium of tubes, r_o is the outer radium of tubes, l is the length of tubes (~3.0 μm), and N_t is the density of hollow cylinder (~5.66 × 10^9 cm^{-2}). Considering the initial surface exhibiting a nominal area of 1 cm^2, the specific area of TNTs is calculated to be ~110 cm^2. The significantly increased specific area provides large surfaces for PEC reaction, leading to an enhanced PEC performance.

The effect of electrochemical reduction on the crystal structure and phase of TNTAs was investigated. Figure 2 exhibits the X-ray diffraction (XRD) patterns of TNTs and −1.5 V-R-TNTs. For the pattern of TNTs, all peaks can be readily indexed to anatase TiO_2 (JCPDF No. 21-1272) except for the peaks at 35.2°, 38.0°, 40.2°, and 77.2° originated from the Ti substrate [28, 29]. As shown in Fig. 2, the strong XRD diffraction peaks for the anatase phase showed no changes, regardless of electrochemical reduction,

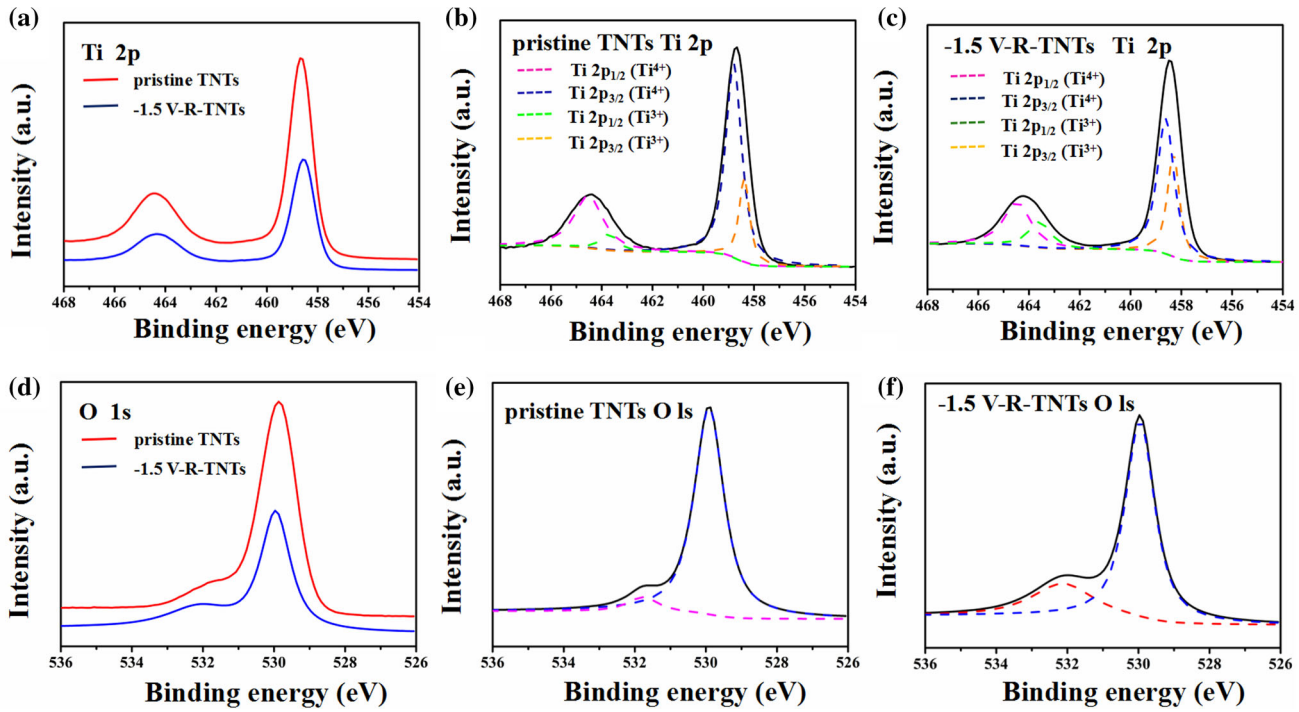

Figure 3 XPS spectra of pristine TNTs and −1.5 V-R-TNTs. **a** Comparison of Ti 2p peak of TNTs before and after electrochemical reduction, **b** Ti 2p in pristine TNTs, **c** Ti 2p in −1.5 V-R-TNTs, **d** comparison of O 1 s peak of TNTs before and after electrochemical reduction, **e** O 1 s in pristine TNTs, **f** O 1 s in −1.5 V-R-TNTs.

Table 1 The fitting parameters of Ti 2p and O 1 s in pristine TNTs

Element		Binding energy (eV)	Half widths (eV)	Intensity × 10^4	Area × 10^4
Ti	Ti^{4+} $2p_{3/2}$	458.5	0.753	6.308	4.750
	Ti^{4+} $2p_{1/2}$	464.5	1.382	1.557	2.152
	Ti^{3+} $2p_{3/2}$	457.9	0.491	2.688	1.321
	Ti^{3+} $2p_{1/2}$	463.7	0.827	0.643	0.532
O	O–Ti–O	529.84	0.985	15.081	14.855
	Ti–OH	531.8	1.117	1.050	1.178

indicating that TNTs maintain their original phase and crystal structure after electrochemical reduction.

The XPS techniques were employed to confirm the reduction of TNTs and identify the element composition and chemical state of the pristine TNTs and −1.5 V-R-TNTs. Figure 3a shows the high resolution XPS spectra of Ti 2p in the samples. As observed, the peaks of Ti 2p in the −1.5 V-R-TNTs exhibit a slight negative shift, which supports the presence of Ti^{3+} states [30, 31]. Upon fitting (Fig. 3c), the two broad peaks centered at about 458.53 and 464.27 eV can be split into four peaks of Ti^{4+} $2p_{1/2}$ (464.5 eV), Ti^{4+} $2p_{3/2}$ (458.5 eV), Ti^{3+} $2p_{1/2}$ (463.7 eV), and Ti^{3+} $2p_{3/2}$ (457.9 eV). The fitting parameters (half widths, intensity, and area) of Ti 2p in the pristine TNTs and −1.5 V-R-TNTs are listed in Tables 1 and 2. It can be observed that the $Ti^{4+}/Ti^{3}+$ intensity ratio for the $2p_{3/2}$ and $2p_{1/2}$ in Fig. 3b, c is ∼2.346, ∼2.452, ∼1.266, and ∼1.298, respectively. Compared with the Ti^{4+}/Ti^{3+} intensity ratio of the pristine TNTs, the intensity ratio of −1.5 V-R-TNTs shows an obvious decrease, indicating a high concentration of Ti^{3+} defects formed during electrochemical reduction process. As shown in Fig. 3d, a shoulder peak centered at 529.84 eV with high intensity can be clearly observed for both samples, which is attributed to the characteristic peak of Ti–O–Ti species. The peak at 531.8 eV shows an obvious increase after electrochemical reduction, which can be attributed to the formation of the hydroxyl group on the surface of

Table 2 The fitting parameters of Ti 2p and O 1 s in −1.5 V-R-TNTs

Element		Binding energy (eV)	Half widths (eV)	Intensity × 10^4	Area × 10^4
Ti	Ti^{4+} $2p_{3/2}$	458.5	0.677	5.371	3.636
	Ti^{4+} $2p_{1/2}$	464.5	1.264	1.560	1.975
	Ti^{3+} $2p_{3/2}$	457.9	0.567	4.241	2.405
	Ti^{3+} $2p_{1/2}$	463.7	0.788	1.201	0.947
O	O–Ti–O	529.84	0.990	7.822	7.744
	Ti–OH	531.80	2.100	1.307	2.745

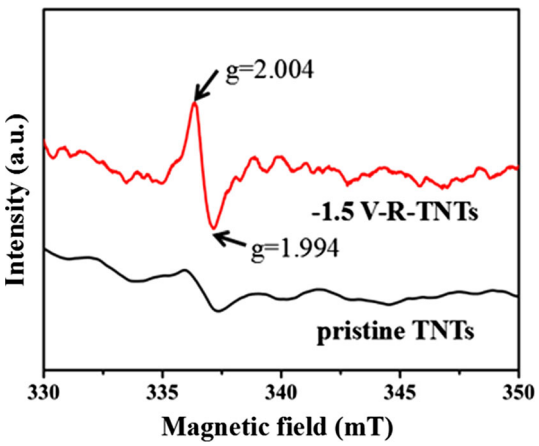

Figure 4 EPR spectra of *a* pristine TNTs and *b* −1.5 V-R-TNTs.

TiO_2 [32]. Figure 3e and f shows the fitted spectra of O 1 s in TNTs before and after reduction, which corresponds to Ti–O–Ti (529.91 eV) and Ti–OH (531.77 eV) peaks [33, 34]. From the fitted results, it is observed that the content of hydroxyl groups increased after TiO_2 reduction.

To further verify the presence of Ti^{3+} and oxygen vacancies in the TNTs, low-temperature EPR spectra were performed on the pristine TNTs and −1.5 V-R-TNTs, shown in Fig. 4. It can be observed that the pristine TNTs present very weak EPR signals. In contrast, the −1.5 V-R-TNTs sample shows strong signals at *g* value of 2.004 and 1.994, corresponding to oxygen vacancy and Ti^{3+}, which is consistent with the results reported by Zhu et al. [19]. The findings from EPR spectra characterization suggest that electrochemical reduction method can induce Ti^{3+} and oxygen vacancies into the TNTs.

PEC measurements were performed to assess the photoelectrochemical properties of TNTs before and after electrochemical reduction. To investigate the effect of reduction duration on the PEC performance of TNTs, reduced TNTs at −1.5 V for different times (5, 10, and 20 min) were prepared. Figure 5a shows a set of linear sweep voltammograms (LSV) recorded from pristine TNTs and reduced TNTs for different times under AM 1.5 G illumination (100 mW cm^{-2}). It can be observed that the photocurrent density of TNTs first increased with the reduction time and reached a maximum value after reduction for 10 min, and then decreased with the reduction time further increasing. The applied cathodic potential in the reduction process exhibits a similar influence on the PEC performance of reduced TNTs, which is shown in Fig. 5c. The lower photocurrent density of TNTs reduced at higher potentials (−1.8 V) or for longer reduction duration (20 min) can be ascribed to the increased recombination centers after inducing excessive Ti^{3+} or oxygen vacancies into the lattice of TiO_2 by electrochemical reduction [30], which is similar to the TNTs modified by metal or nonmetal doping [6, 35].

To further investigate the photoresponse of the samples, the transient photocurrent response measurements were carried out during repeated on–off solar light illumination cycles at 0.6 V versus Ag/AgCl (Fig. 5b, d). It is found that reduced TNTs at −1.5 V for 10 min are an optimum for enhanced PEC performance. Under AM 1.5 G illumination, the photocurrent of reduced TNTs exhibits a higher photocurrent of 0.525 mA cm^{-2} at 0.6 versus Ag/AgCl, which is 3.1 times that of the pristine TNTs (0.170 mA cm^{-2}).

Figure 6a presents the plots of the photoconversion efficiencies versus applied bias potentials of the pristine TNTs and −1.5 V-R-TNTs. The pristine TNTs achieved a maximum photoconversion efficiency of 0.12% at −0.54 V (vs Ag/AgCl), while the optimal photoconversion efficiency can up to 0.21% at a higher bias of −0.33 V (vs Ag/AgCl) for reduced TNTs, which is about 1.75 times larger than the values obtained on pristine TNTs. The stability of the samples was investigated at 0.6 V versus Ag/AgCl under continuous AM 1.5 G illumination for 60 min, and the results are presented in Fig. 6b. It is clearly

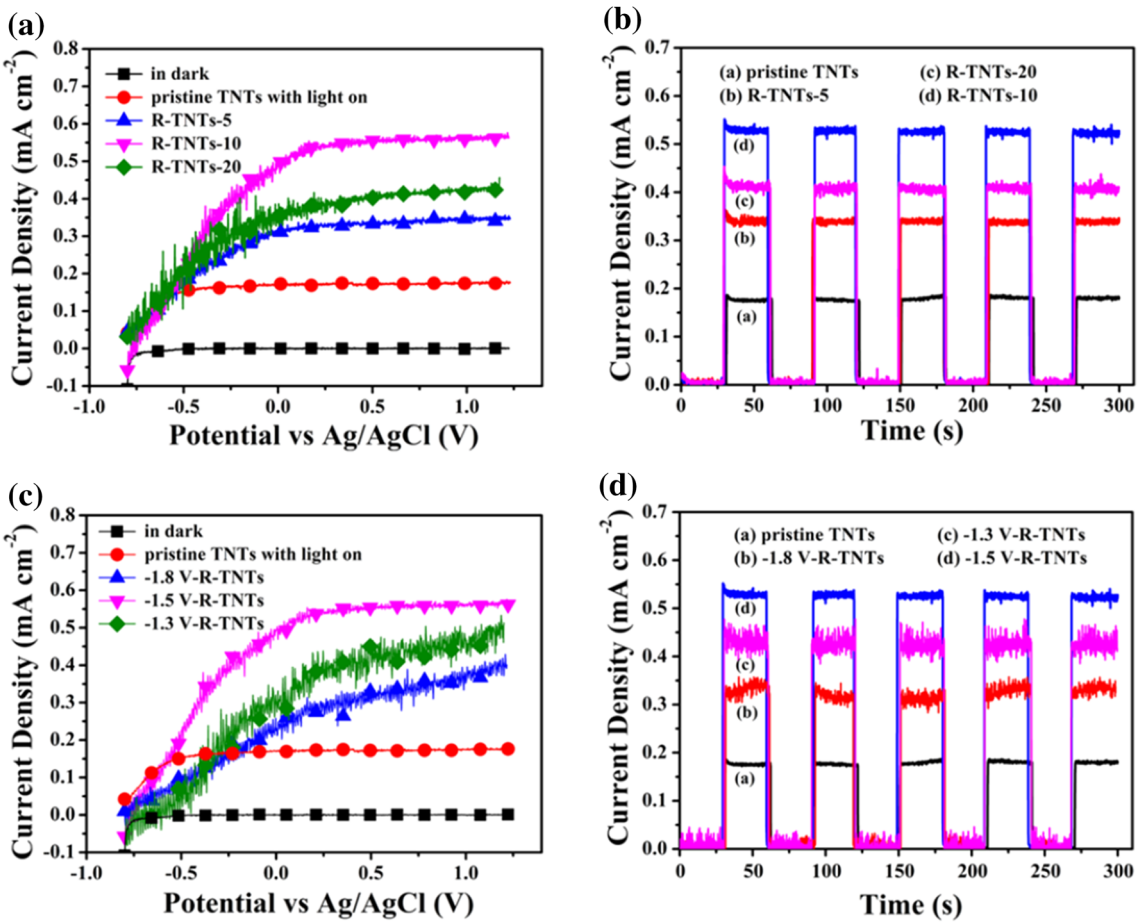

Figure 5 PEC performance of TNTs before and after electrochemical reduction was measured under AM 1.5 G illumination. Linear sweep voltammograms of samples prepared at −1.5 V for different reduction duration (**a**) and prepared at different reduction potentials for 10 min (**c**). Amperometric transient current density versus time plots recorded from samples prepared at −1.5 V for different reduction duration (**b**) and prepared at different reduction potentials for 10 min (**d**) at an applied potential of 0.6 V versus Ag/AgCl with 30-s light on–off cycles.

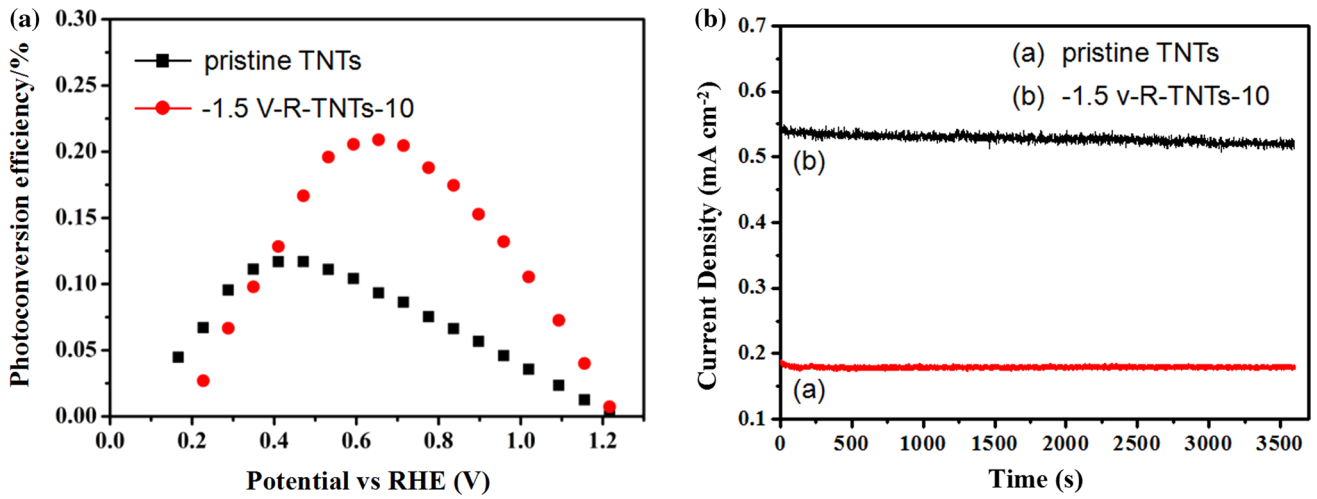

Figure 6 **a** Photoconversion efficiency of pristine TNTs and −1.5 V-R-TNTs-10 as a function of applied potential. **b** Stability of pristine TNTs and −1.5 V-R-TNTs-10; the photocurrent was collected at 0.6 V versus Ag/AgCl under 1.5 G illumination.

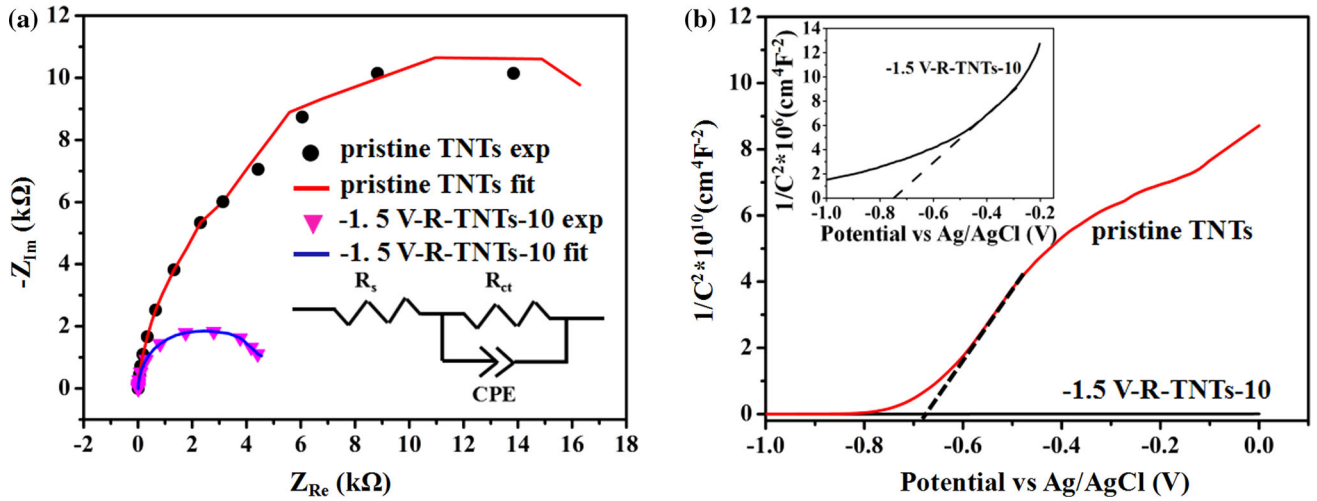

Figure 7 **a** Nyquist plots collected at open-circuit potential under light illumination, where the *scatter points* in the plots represent the original experimental data, and the *solid lines* are the fitted curves using the equivalent circuit model in the *inset* of Fig. 6a. **b** Mott–Schottky plots of pristine TNTs and −1.5 V-R-TNTs-10 collected at a frequency of 1 kHz in the dark.

observed that the photocurrent density of both samples did not show any significant decay, exhibiting a good stability. It is well known that the pristine TNTs present high photochemical stability during PEC measurements, which is important for photoelectrodes [36]. For electrochemical reduced TNTs, the good stability of PEC performance shows that Ti^{3+} in the TNTs is stable, which is also demonstrated in the paper reported by Zhang et al. [11].

Electrochemical impedance spectra (EIS) measurement is a powerful tool for studying the interfacial properties between electrodes and solution [37]. Figure 7a presents the Nyquist plots for the pristine TNTs and −1.5 V-R-TNTs under illumination condition, where the scatter points in the plots represent the original experimental data, and the solid lines are the fitted curves using the equivalent circuit model in the inset of Fig. 7a. As indicated, the equivalent circuit model fitted well with both of the samples. In our model, R_s represents the overall series resistance of the circuit, and R_{ct} corresponds to the charge transfer resistance. As depicted in Fig. 7a, the −1.5 V-R-TNTs exhibited a smaller semicircular diameter than the pristine TNTs, indicating that the charge transfer proceeds more easily on the reduced TNTs. The charge transfer resistance can be derived by fitting the Nyquist plots with the equivalent circuit model. As expected, the charge transfer resistance R_{ct} of −1.5 V-R-TNTs is significantly decreased from 22751 (pristine TNTs) to 4985 Ω, suggesting an enhanced charge transfer process in the reduced TNTs and thus a more effective separation of photogenerated electron–hole pairs.

To further study the intrinsic electronic properties of pristine TNTs and −1.5 V-R-TNTs in electrolyte solution, Mott–Schottky (MS) measurements were performed on the samples in dark to determine the capacitance of electrodes. MS plots collected at 1 kHz are presented in Fig. 7b. It can be used to determine the semiconductor type, flat band potential (U_{fb}) at semiconductor/electrolyte interface, and carrier density (N_d) following the equation [26]:

$$\frac{1}{C^2} = \left(\frac{2}{e_0 \varepsilon \varepsilon_0 N_d A^2}\right)\left(U - U_{fb} - \frac{k_B T}{e_0}\right) \quad (2)$$

where C, e_0, ε, ε_0, N_d, A, U, U_{fb}, k_B, and T represent the space charge capacitance, the electron charge, the dielectric constant of semiconductor electrode, the permittivity of the vacuum, the carrier density, the area, the applied potential, the flat band potential, the Boltzmann constant, and the absolute temperature, respectively. As shown in Fig. 7b, the slopes of the MS plots were positive, characteristic of n-type semiconductor, implying that the electrochemical reduction process did not change the semiconductor type of the reduced TNTs. By extrapolating the linear parts of the curves to be $1/C^2 = 0$, the flat band potential can be determined. The values of U_{fb} were estimated to be −0.68 and −0.75 V (vs Ag/AgCl) for pristine TNTAs and −1.5 V-R-TNTs, respectively. The negative shift of U_{fb} indicates a shift of conduction band to more positive potentials [38], which

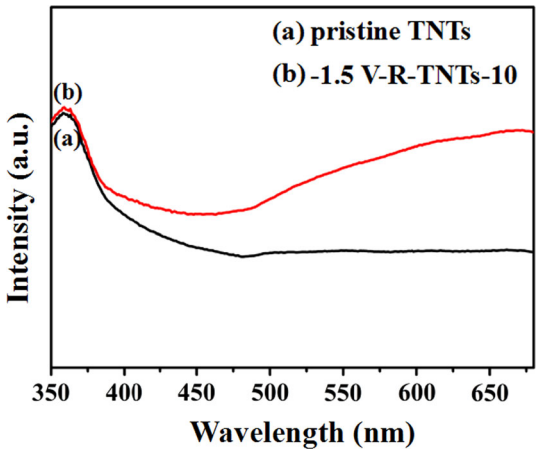

Figure 8 Diffuse reflectance UV–Vis absorption of *a* pristine TNTs, *b* −1.5 V-R-TNTs-10.

leads to enhanced electrical conductivity of the reduced TNTs. The charge density of TNTs before and after electrochemical reduction can be determined by the following equation:

$$N_{\mathrm{d}} = \left(\frac{2}{e_0 \varepsilon \varepsilon_0}\right)\left(\frac{\mathrm{d}\left(1/C^2\right)}{\mathrm{d}U}\right)^{-1}. \quad (3)$$

We take $\varepsilon = 48$ for anatase TiO_2 [11]. As presented in the inset of Fig. 7b, the −1.5 V-R-TNTs showed a much smaller linear slope than that of the pristine TNTs, suggesting an increase of charge density in the reduced TNTs due to the introduction of Ti^{3+} or oxygen vacancies [28]. As calculated, the charge density of −1.5 V-R-TNTs reached a maximum of $\sim 8.833 \times 10^{20}$ cm^{-3}, while the pristine TNTs exhibited a lower charge density of $\sim 1.52 \times 10^{17}$ cm^{-3}. Thus, the electrical conductivity of −1.5 V-R-TNTs could be greatly increased. Moreover, the expected upward shift of the Fermi level caused by the increased electron density can lead to a larger degree of band bending at the surface of the reduced TNTs, which could promote the charge separation at the semiconductor/electrolyte interface [37, 39]. Therefore, the improved charge transport, along with the facilitated charge separation, is responsible for the enhanced PEC performance.

The diffuse reflectance UV–Vis absorption spectra of the TNTs before and after electrochemical reduction are shown in Fig. 8. Compared with the pristine TNTs, the reduced TNTs show a dramatically enhanced light absorption in the visible light region of the spectrum, which is consistent with the previous reports [40, 41], while it exhibits a slight enhancement in the UV region, which is in accordance with the results reported by Liao et al. [30]. Based on a previous report [11], a series of Ti^{3+} interstitial bands are formed with energies 0.27 to 0.87 eV below the conduction band minimum of TiO_2, leading to the band gap narrowing for the reduced TNTs. The strong absorption of the reduced sample is due to the additional transitions between the different energy levels of the Ti^{3+} states, oxygen vacancies, conduction band, and valence band [42]. The enhanced light absorption contributed to the enhanced PEC performance, which is in line with the results demonstrated in Figs. 5 and 6.

Conclusions

In summary, Ti^{3+}-self-doped TNTs were fabricated by simple electrochemical reduction method and used as photoanode of photoelectrochemical cells for water splitting. It is noteworthy to mention that the structure of TNTs did not show any change after reduction process, suggesting that the morphology of TNTs was stable and not undergoing any destruction under electrochemical reduction. By controlling the electrochemical reduction duration and potential, a high photocurrent density of ~ 0.525 mA cm^{-2} was obtained, which is nearly 3.1 times higher than pristine TNTs. Compared with the pristine TNTs, the flat band potential of Ti^{3+}-self-doped TNTs exhibited a negative shift, which could effectively facilitate the charge transfer. Besides, the PEC response to visible light region was demonstrated to be greatly enhanced. Therefore, the excellent PEC performance of reduced TNTs can be attributed to the increased charge density, fast electron–hole separation, and improved visible light absorption, as confirmed by XPS, impedance analysis, and UV–Vis diffuse reflection spectra.

Acknowledgements

This work was supported by National 863 Program [Grant Number 2011AA050518]; the Natural Science Foundation of China [Grant Numbers 11174197, 11574203, 61234005]; laboratory of Crime Scene Evidence Program [Grant Number 2014XCWZK02].

References

[1] Fujishima A, Honda K (1972) TiO_2 photoelectrochemistry and photocatalysis. Nature 238:37

[2] Chetibi L, Hamana D, Achour A, Achour S, Peszke J (2014) Hydroxyapatite growth on multiwall carbon nanotubes grown on titanium fibers from a titanium sheet. J Mater Sci 49:621–632. doi:10.1007/s10853-013-7742-6

[3] Zhu C, Li C, Zheng M, Delaunay JJ (2015) Plasma-induced oxygen vacancies in ultrathin hematite nanoflakes promoting photoelectrochemical water oxidation. Acs Appl Mater Interfaces 7:22355–22363

[4] Li C, Hisatomi T, Watanabe O, Nakabayashi M, Shibata N, Domen K, Delaunay JJ (2015) Positive onset potential and stability of Cu_2O-based photocathodes in water splitting by atomic layer deposition of a Ga_2O_3 buffer layer. Energy Environ Sci 8:1493–1500

[5] Jiao J, Tang J, Gao W, Kuang D, Tong Y, Chen L (2015) Plasmonic silver nanoparticles matched with vertically aligned nitrogen-doped titanium dioxide nanotube arrays for enhanced photoelectrochemical activity. J Power Sources 274:464–470

[6] Li J, Liu CL, Ye YF, Zhu JF, Wang SD, Guo JH, Sham TK (2016) Tracking the local effect of fluorine self-doping in anodic TiO_2 nanotubes. J Phys Chem C 120:4623–4628

[7] Moon J (2001) Preparation and characterization of the Sb-doped TiO_2 photocatalysts. J Mater Sci 36:949–955. doi:10.1023/A:1004819706292

[8] Altomare M, Lee K, Killian MS, Selli E, Schmuki P (2013) Ta-doped TiO_2 nanotubes for enhanced solar-light photoelectrochemical water splitting. Chem Eur J 19:5841–5844

[9] Kang Q, Cao J, Zhang Y, Liu L, Xu H, Ye J (2013) Reduced TiO_2 nanotube arrays for photoelectrochemical water splitting. J Mater Chem A 1:5766–5774

[10] Tan H, Zhao Z, Niu M, Mao C, Cao D, Cheng D, Feng P, Sun Z (2014) A facile and versatile method for preparation of colored TiO_2 with enhanced solar-driven photocatalytic activity. Nanoscale 6:10216–10223

[11] Zhang Z, Hedhili MN, Zhu H, Wang P (2013) Electrochemical reduction induced self-doping of Ti^{3+} for efficient water splitting performance on TiO_2 based photoelectrodes. Phys Chem Chem Phys 15:15637–15644

[12] Cui XF, Jiang GY, Zhao Z, Xu CM, Bai WK, Wang JY, Duan AJ, Liu J, Wei YC (2016) Facile regulation of crystalline phases and exposed facets on Ti^{3+} self-doped TiO_2 for efficient photocatalytic hydrogen evolution. J Mater Sci 51:10819–10832. doi: 10.1007/s10853-016-0293-x

[13] Fujino T, Katayama M, Inudzuka K, Okuno T, Oura K, Hirao T (2001) Surface hydroxyl formation on vacuum-annealed TiO_2 (110). Appl Phys Lett 79:2716–2718

[14] Lu H, Zhao B, Pan R, Yao J, Qiu J, Luo L, Liu Y (2014) Safe and facile hydrogenation of commercial Degussa P25 at room temperature with enhanced photocatalytic activity. RSC Adv 4:1128–1132

[15] Liu N, Schneider C, Freitag D, Hartmann M, Venkatesan U, Muller J, Spiecker E, Schmuki P (2014) Black TiO_2 nanotubes: cocatalyst-free open-circuit hydrogen generation. Nano Lett 14:3309–3313

[16] Wang J, Yang P, Huang B (2015) Self-doped TiO_{2-x} nanowires with enhanced photocatalytic activity: facile synthesis and effects of the Ti^{3+}. Appl Surf Sci 356:391–398

[17] Ihara T, Miyoshi M (2001) Preparation of a visible-light-active TiO_2 photocatalyst by RF plasma treatment. J Mater Sci 36:4201–4207. doi: 10.1023/A:1017929207882

[18] Li J, Liu CH, Li X, Wang ZQ, Shao YC, Wang SD, Sun XL, Pong WF, Guo JH, Sham TK (2016) Unraveling the origin of visible light capture by core-shell TiO_2 nanotubes. Chem Mater 28:4467–4475

[19] Zhu G, Lin T, Lü X, Zhao W, Yang C, Wang Z, Yin H, Liu Z, Huang F, Lin J (2013) Black brookite titania with high solar absorption and excellent photocatalytic performance. J Mater Chem A 1:9650–9653

[20] Hou X, Shang M, Bi Y, Jiao Z (2016) Synthesis of Ti^{3+} self-doped $SrTiO_3/TiO_2$ hetero-photoanodes with enhanced photoelectrochemical performances under visible light. Mater Lett 176:270–273

[21] Si L, Huang ZA, Lv K, Tang D, Yang C (2014) Facile preparation of Ti3 + self-doped TiO2 nanosheets with dominant 001 facets using zinc powder as reductant. J Alloys Compd 601:88–93

[22] Zuo F, Wang L, Feng P (2014) Self-doped Ti^{3+}@TiO_2 visible light photocatalyst: influence of synthetic parameters on the H_2 production activity. Int J Hydrogen Energy 39:711–717

[23] Chang YH, Liu CM, Chen C, Cheng HE (2012) The effect of geometric structure on photoluminescence characteristics of 1-D TiO_2 nanotubes and 2-D TiO_2 films fabricated by atomic layer deposition. J Electrochem Soc 159:D401–D405

[24] Chang X, Thind SS, Chen A (2014) Electrocatalytic enhancement of salicylic acid oxidation at electrochemically reduced TiO_2 nanotubes. ACS Catal 4:2616–2622

[25] Close T, Tulsyan G, Diaz CA, Weinstein SJ, Richter C (2015) Reversible oxygen scavenging at room temperature using electrochemically reduced titanium oxide nanotubes. Nature nanotech 10:418–422

[26] Li Q, Zheng M, Zhang B, Zhu C, Wang F, Song J, Zhong M, Ma L, Shen W (2016) InP nanopore arrays for photoelectrochemical hydrogen generation. Nanotechnology 27: 075704–075714

[27] Li Z, Ding Y, Kang W, Li C, Lin D, Wang X, Chen Z, Wu M, Pan D (2015) Reduction mechanism and capacitive properties of highly electrochemically reduced TiO_2 nanotube arrays. Electrochim Acta 161:40–47

[28] Cui H, Zhao W, Yang C, Yin H, Lin T, Shan Y, Xie Y, Gu H, Huang F (2014) Black TiO_2 nanotube arrays for high-efficiency photoelectrochemical water-splitting. J Mater Chem A 2:8612–8616

[29] Wu H, Li D, Zhu X, Yang C, Liu D, Chen X, Song Y, Lu L (2014) High-performance and renewable supercapacitors based on TiO_2 nanotube array electrodes treated by an electrochemical doping approach. Electrochim Acta 116:129–136

[30] Liao W, Yang J, Zhou H, Murugananthan M, Zhang Y (2014) Electrochemically self-doped TiO_2 nanotube arrays for efficient visible light photoelectrocatalytic degradation of contaminants. Electrochim Acta 136:310–317

[31] Kim C, Kim S, Lee J, Kim J, Yoon J (2015) Capacitive and oxidant generating properties of black-colored TiO_2 nanotube array fabricated by electrochemical self-doping. ACS Appl Mater Interfaces 7:7486–7491

[32] Zhang T, Cui S, Yu B, Liu Z, Wang D (2015) Surface engineering for an enhanced photoelectrochemical response of TiO_2 nanotube arrays by simple surface air plasma treatment. Chem Commun 51:16940–16943

[33] Zhou H, Zhang Y (2014) Electrochemically self-doped TiO_2 nanotube arrays for supercapacitors. J Phys Chem C 118:5626–5636

[34] Pan X, Xu YJ (2013) Defect-mediated growth of noble-metal (Ag, Pt, and Pd) nanoparticles on TiO_2 with oxygen vacancies for photocatalytic redox reactions under visible light. J Phys Chem C 117:17996–18005

[35] Choi H, Shin D, Yeo BC, Song T, Han SS, Park N, Kim S (2016) Simultaneously controllable doping sites and the activity of a W-N codoped TiO2 photocatalyst. ACS Catal 6:2745–2753

[36] Bakar SA, Ribeiro C (2016) Low temperature synthesis of N-doped TiO_2 with rice-like morphology through peroxo assisted hydrothermal route: materials characterization and photocatalytic properties. Appl Surf Sci 377:121–133

[37] Shang MD, Hu HY, Lu GX, Bi YP (2016) Synergistic effects of $SrTiO_3$ nanocubes and Ti^{3+} dual-doping for highly improving photoelectrochemical performance of TiO_2 nanotube arrays under visible light. J Mater Chem A 4:5849–5853

[38] Kontos AI, Likodimos V, Stergiopoulos T, Tsoukleris DS, Falaras P (2009) Self-organized anodic TiO_2 nanotube arrays functionalized by iron oxide nanoparticles. Chem Mater 21:662–672

[39] Hu S, Shaner MR, Beardslee JA, Lichterman M, Brunschwig BS, Lewis NS (2014) Amorphous TiO_2 coatings stabilize Si, GaAs, and GaP photoanodes for efficient water oxidation. Science 344:1005–1009

[40] Ghicov A, Tsuchiya H, Hahn R, Macak JM, Muñoz AG, Schmuki P (2006) TiO_2 nanotubes: H^+ insertion and strong electrochromic effects. Electrochem Commun 8:528–532

[41] Tokudome H, Miyauchi M (2005) Electrochromism of titanate-based nanotubes. Angew Chem 44:1974–1977

[42] Zheng Z, Huang B, Meng X, Wang J, Wang S, Lou Z, Wang Z, Qin X, Zhang X, Dai Y (2013) Metallic zinc-assisted synthesis of Ti^{3+} self-doped TiO_2 with tunable phase composition and visible-light photocatalytic activity. Chem Commun 49:868–870